Journal of Geophysical Research: Solid Earth

Supporting Information for

The elusive role of a deep-seated low-angle normal fault activated by the M_w 9.0 Tohoku-Oki megathrust in the triggering of a normal faulting earthquake sequence in northeast Japan

Yohai Magen[1,2], Asaf Inbal[1], Alon Ziv[1], Gidon Baer[2], Roland Burgmann[3], Axel Periollat[4], and Takeshi Sagiya[5]

[1] Department of Geophysics, Tel-Aviv University, Tel Aviv, Israel

[2] Geological Survey of Israel, Jerusalem, Israel

[3]Department of Earth and Planetary Science, University of California Berkeley, Berkeley, CA, USA

[4] Univ. Grenoble Alpes, Univ. Savoie Mont Blanc, CNRS, IRD, Univ. Gustave Eiffel, ISTerre, 38000 Grenoble, France

[5] Disaster Mitigation Research Center, Nagoya University, Nagoya, Japan

Table of content:

- Figure S5. Summary of the 10000 MCMC inversion test results.
- Figure S6, Geometry inversion comparisons using 2, 5 and 10 singular modes.
- Figure S7. Data-to-model misfit as a function of model roughness.
- Figure S8: Modeled coseismic-free strain in IFPB due to aseismic slip along the Mw>5.5 earthquakes faults
- Figure S9. Changes in the CFF along the March 19th earthquake fault
- Figure S10. Changes in the CFF along the March 23rd earthquake fault
- Figure S11. Changes in the CFF along the Iwaki earthquake fault
- Figure S12: Checkerboard resolution test for the low angle normal faults.
- Figure S13: Earthquake distribution in northeast Japan between November 2016 and December 2021
- Table S1. Locations and station codes of the GNSS stations used in this study.
- Table S2. The co-seismic free strain data.

Supporting text 1: Uncertainty Estimation for Strain Data

The robustness of our results depends on the precise estimation of uncertainties associated with the calculated strain data. This section outlines the methodology used for this uncertainty estimation.

To determine the uncertainties linked to the calculated strain data, an empirical approach was employed. We randomly selected 10000 time periods, each spanning 1-30 days, within the two years preceding the Tohoku-Oki earthquake(TOE) (from March 12, 2009, to March 11, 2011). Given the assumption that the strain in the IFPB region should be near zero over such short durations prior to the TOE, these intervals serve as an apt benchmark for uncertainty assessment.

For each of these 10000 intervals, we applied the identical data processing and strain calculation scheme as detailed in the main text. This procedure involved correcting for long-term secular motion, semi-annual, and annual motions, and extracting the local strain fields using GNSS triplets and solving for Equation 3. Then, for each time period, we performed the SVD calculation considering the first 10 singular modes for the final strain data. Each of these random intervals was treated as an independent experiment to assess the variability and potential uncertainty in the calculated strain data.

Upon completing the processing for all 10000 intervals, we computed the standard deviation (std) of the strain values. Multiplying the std by 2 provides an estimate of the uncertainty in the strain data. The underlying rationale is that any deviation from zero in the calculated strain over these short intervals can be attributed to the uncertainty inherent in the data processing and strain calculation procedures.

The derived uncertainties, represented by the std value over the 10000 calculations, are presented in Figure S4 as a function of the GNSS triplet longitude. The strain in the 30 days following the TOE is above the noise level for triplets with a centred longitude>140.35°.

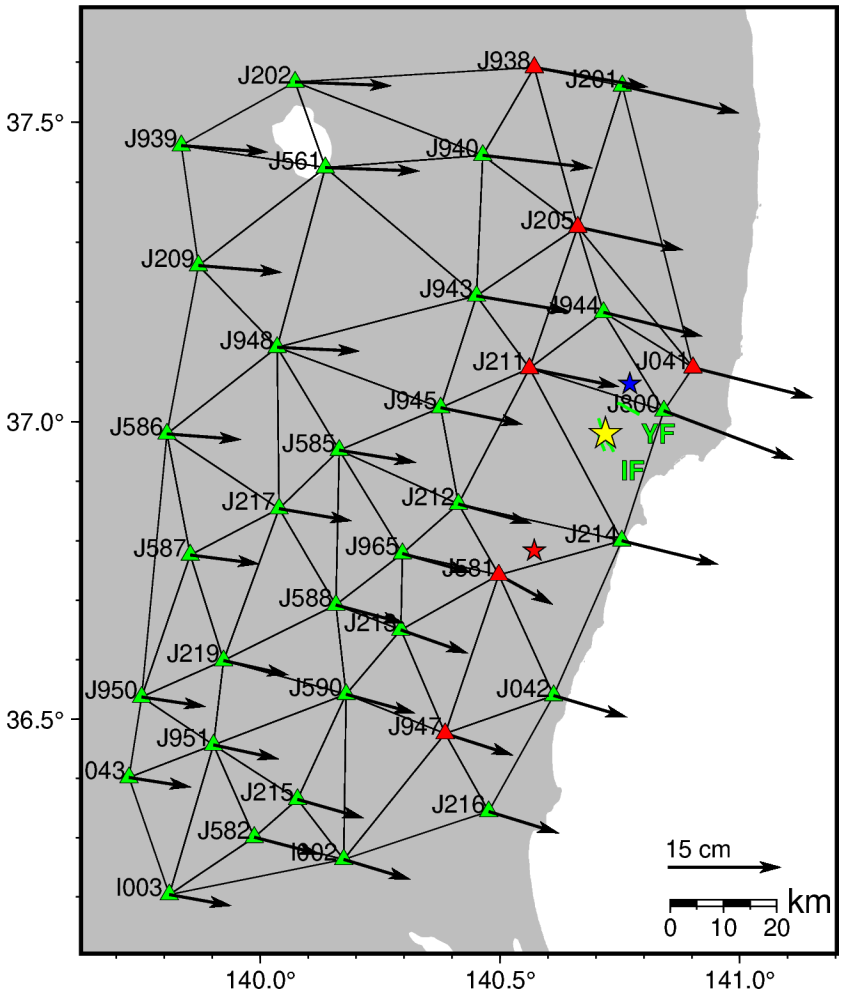

Figure S1

A map showing Japan's GEONET stations used in this study. The triangular mesh indicates the GNSS triplets used for the strain calculation. The red symbols mark the GNSS stations for which time series are shown in Figure S2 and Figure 2. Epicenters of the three M_w>5.6 are indicated by the yellow stars, and the green lines mark fault traces. IF: Itozawa fault ; YF: Yunodake fault.

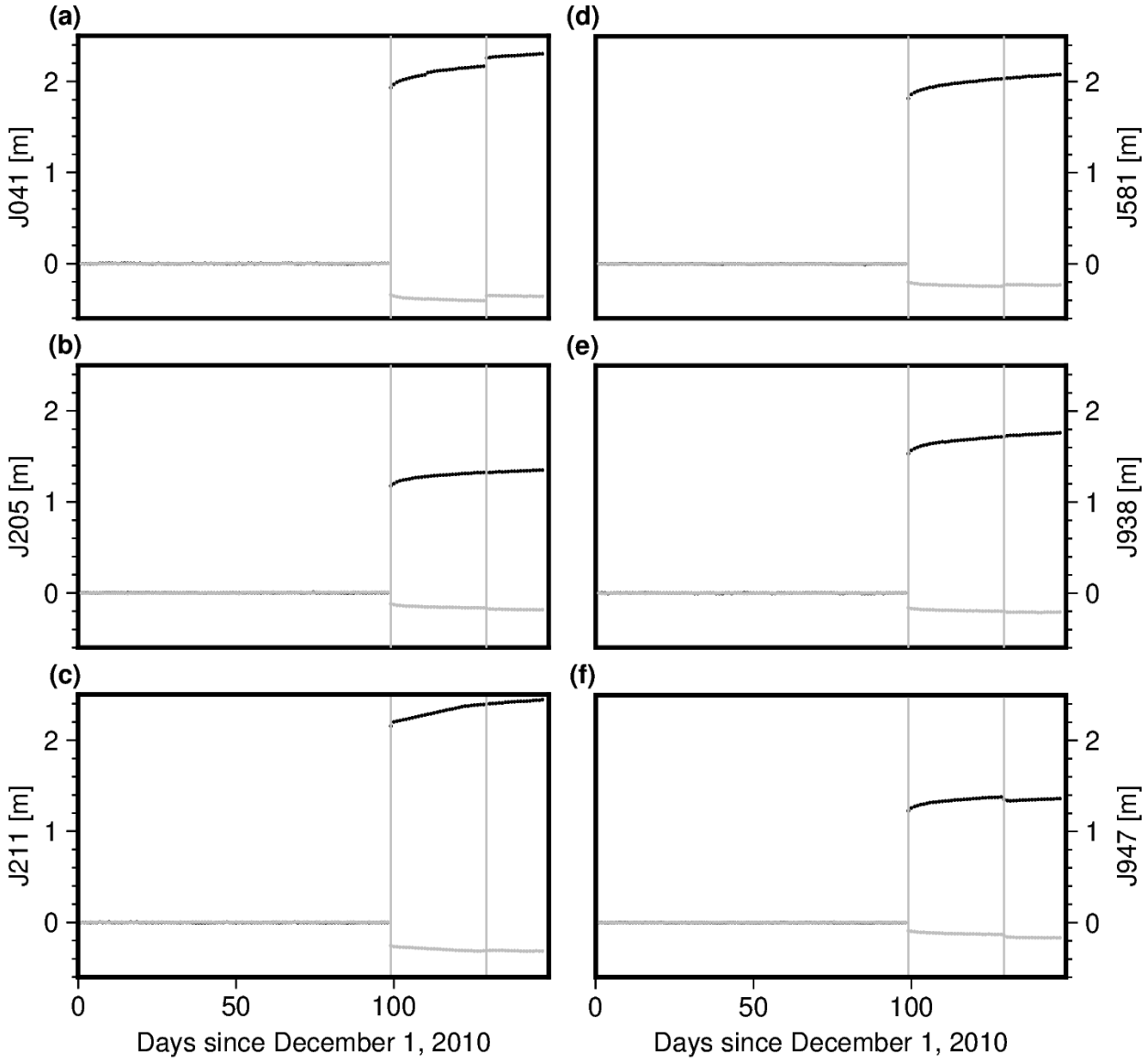

Figure S2

Position time series of GNSS stations for a five-month-long interval between December 1st, 2010 and May 1st, 2011. Station locations are indicated by red triangles in Figure S1. The time series are dominated by the TOE coseismic and postseismic deformation signals. The vertical gray lines indicate the interval analyzed in this study, starting from March 12th, 2011, one day after the TOE mainshock, and ending on April 10, 2011, the day before the M_w6.7 Iwaki earthquake. Black and light gray curves are for east-west and north-south displacement components, respectively.

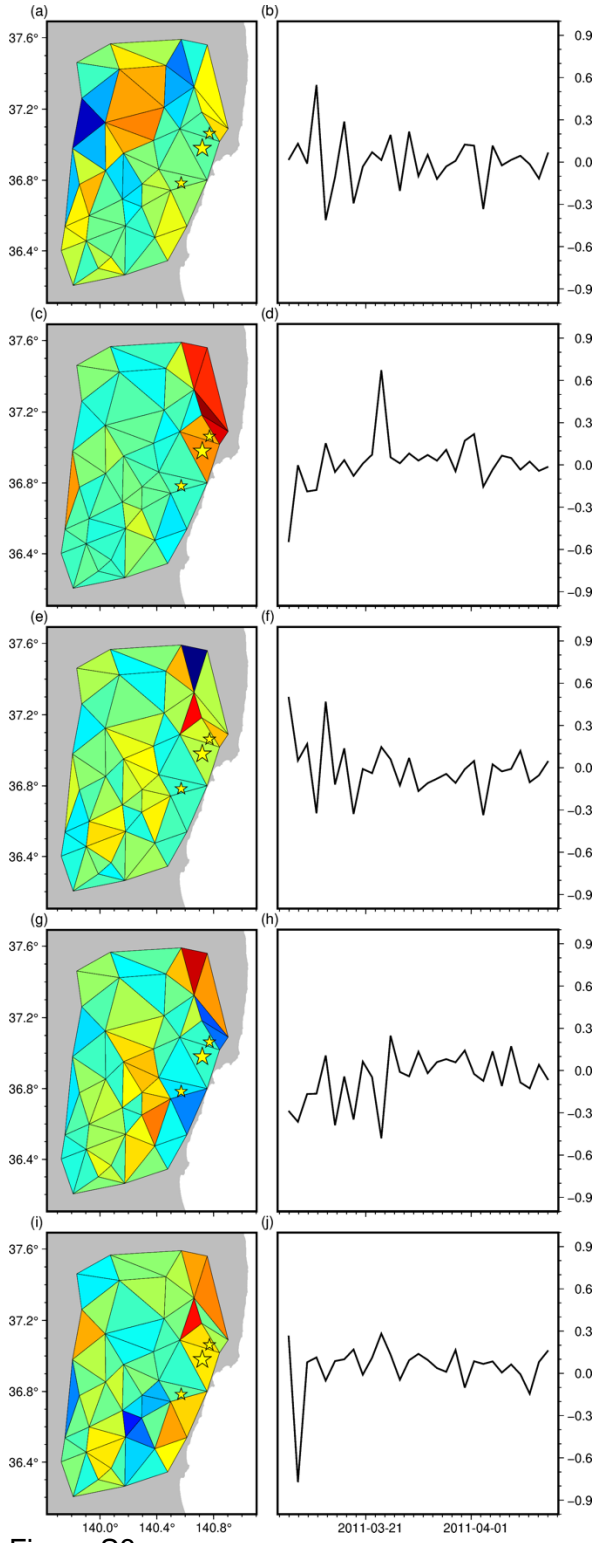

Figure S3.
The coseismic-free strain SVD modes. The left column displays the spatial modes, while the right column exhibits the temporal modes. Each row corresponds to a different mode: (a, b) mode 1, (c, d) mode 2, (e, f) mode 3, (g, h) mode 4, and (i, j) mode 5

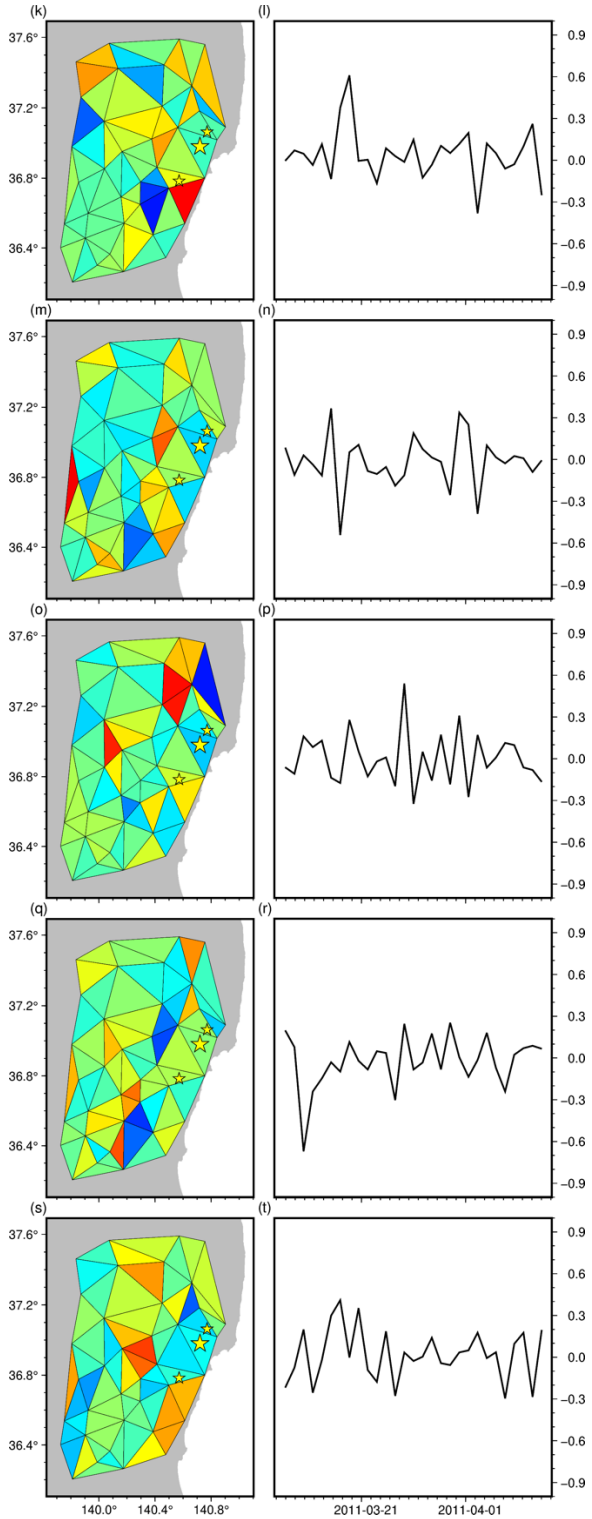

Figure S3 continues.
(k, l) mode 6, (m, n) mode 7, (o, p) mode 8, (q, r) mode 9, and (s, t) mode 10

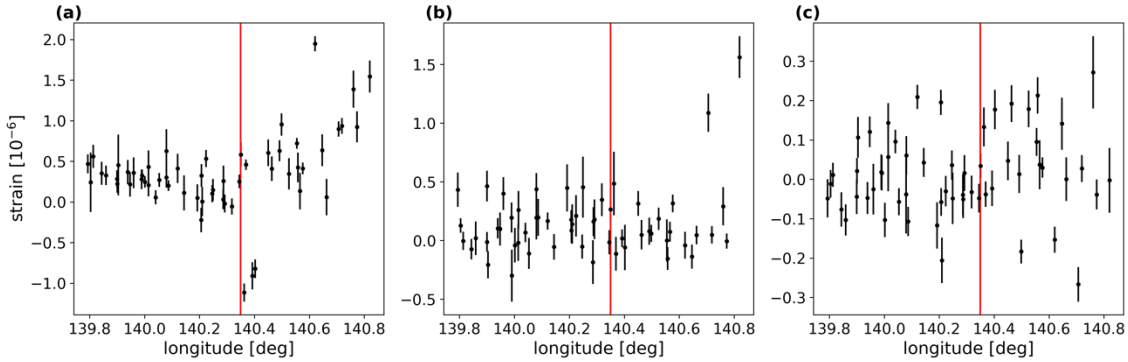

Figure S4

The derived uncertainties in strain data as a function of the GNSS triplet longitude(See Supplementary Text1). The x-axis represents the centered longitude of the GNSS triplets, and the y-axis represents the calculated strain with their respective uncertainties. (a) xx strain, (b) yy strain (c) xy strain

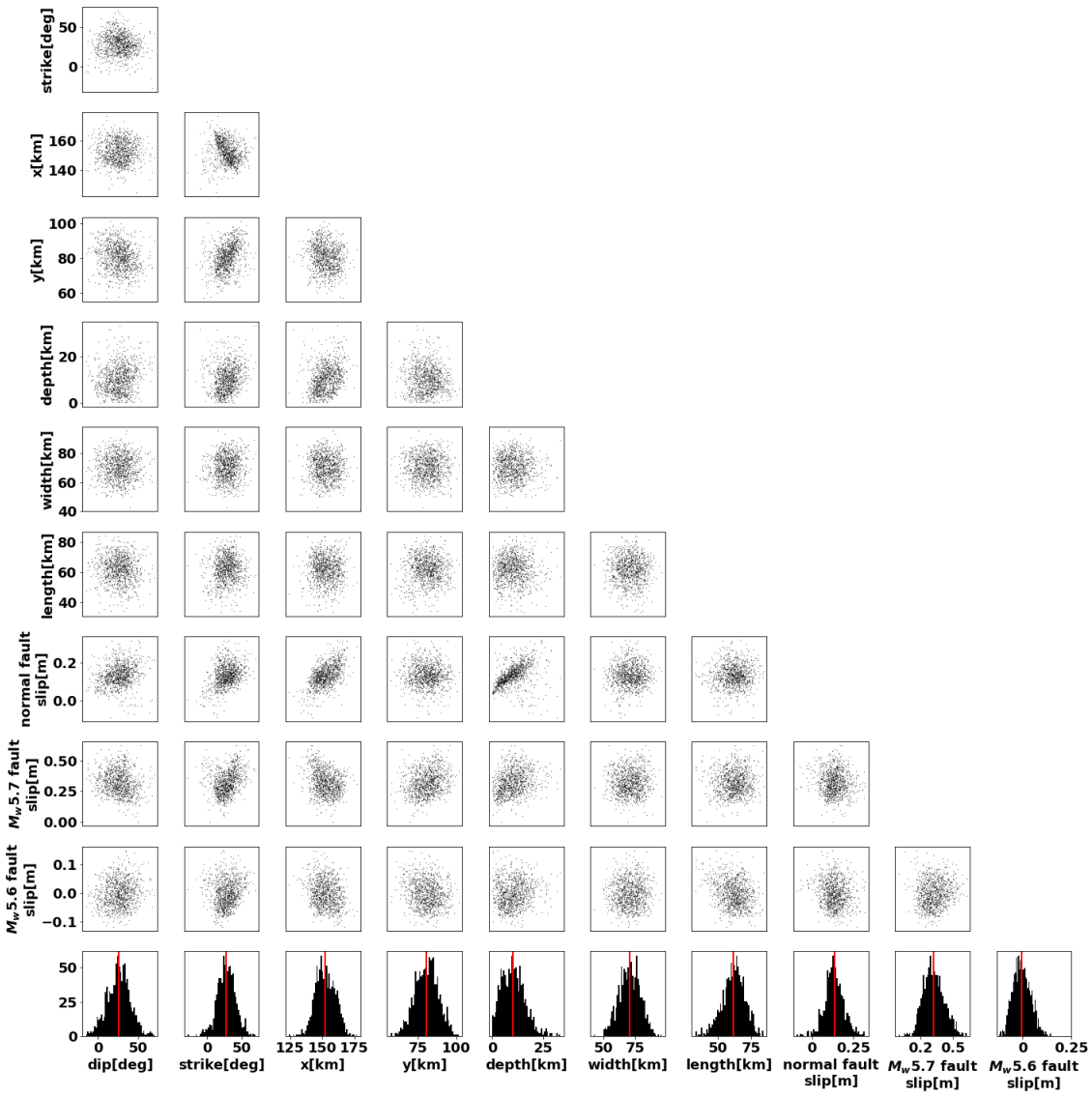

Figure S5

Results of 10^4 MCMC tests for the geometry and slip explaining the inferred strain field. The histograms at the bottom show the distribution of residuals between the observed and modeled strains (see Section 4.1), the eight low-angle normal fault parameters (fault geometry, location, and slip amplitude), and the pre- and post-seismic slip amplitudes of the March 19th M_w5.7 and the March 23rd M_w*5.6* earthquakes. The diagrams on the grid show tradeoffs and interdependencies among the model parameters. X, and Y indicate east-west and north-south distances of the dislocation upper left corner relative to 36°N and 139°E, and depth relates to sea level. Note the strong trade-off between the low-angle normal fault depth and slip amplitude.

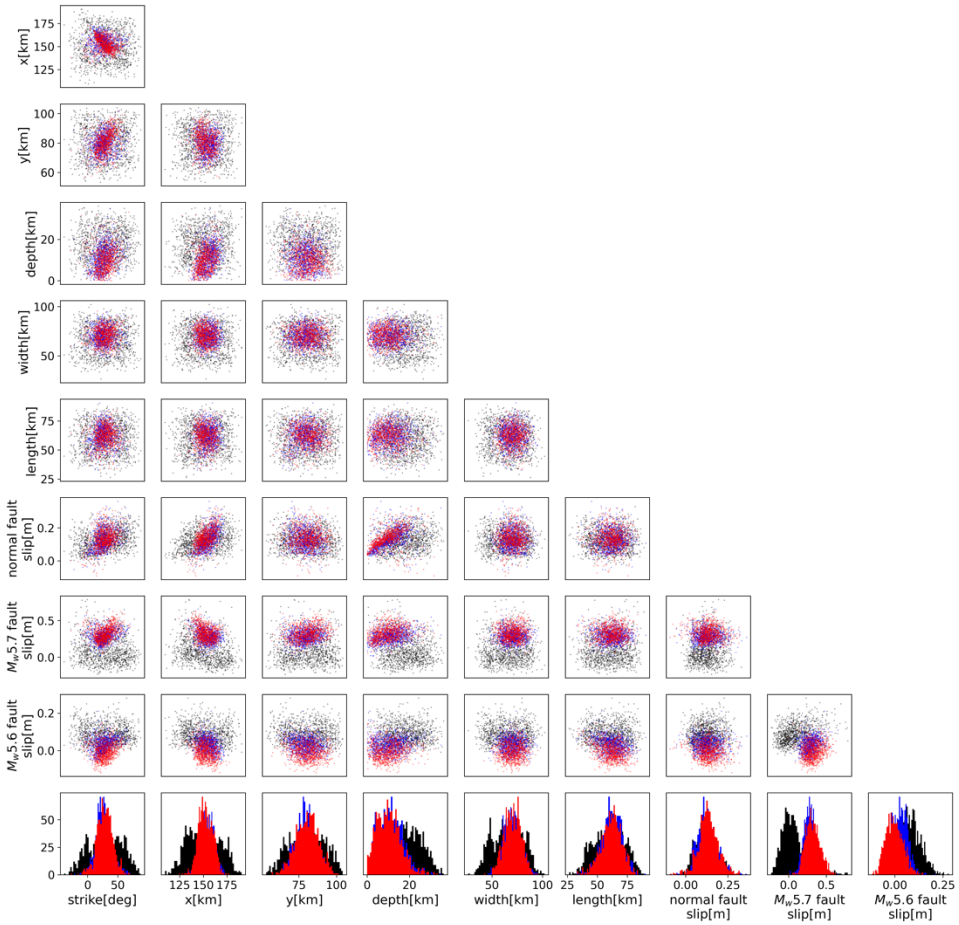

Figure S6. comparison between the geometry inversion results with different singular modes (refer to the first inversion step in section 4.1 of the main text). The black color represents the inversion of strain retrieved from the first two singular modes, accounting for 41% of the variance in the strain data. The blue color represents the strain derived by considering the first five modes of the strain data SVD, accounting for 79% of the data variance. The red color indicates the inversion of strain retrieved from the first ten singular modes (as in Figure S3), accounting for 90% of the variance in the strain data.

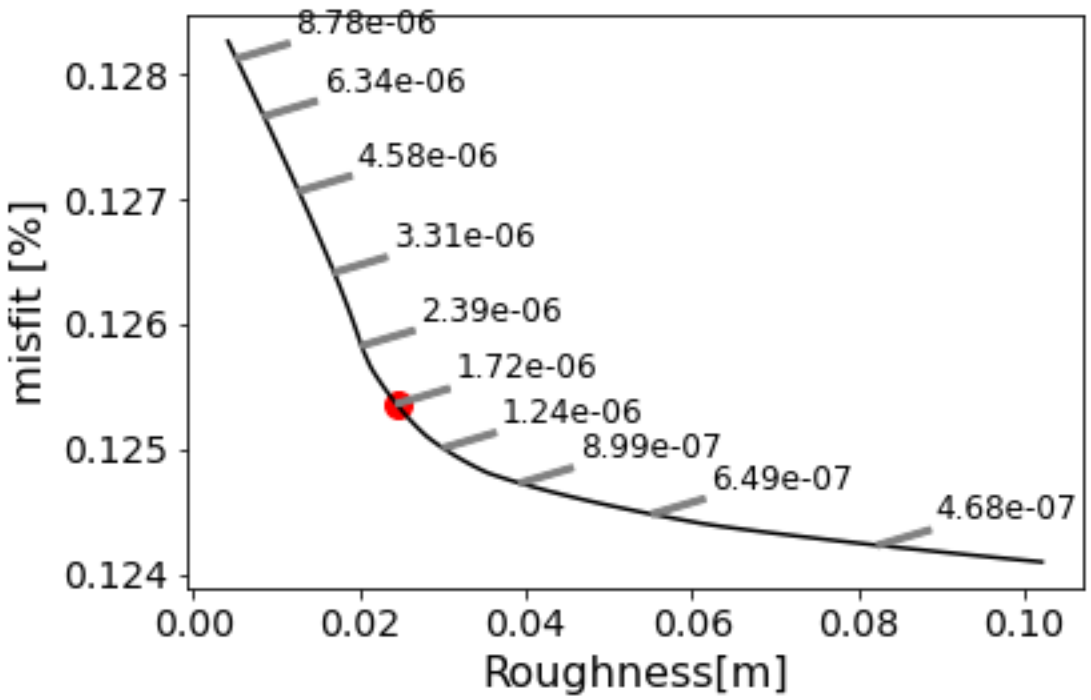

Figure S7. Data-to-model misfit as a function of model roughness ($Roughness = |\nabla m|_2$). The red point shows the inflection point and chosen smoothing coefficient.

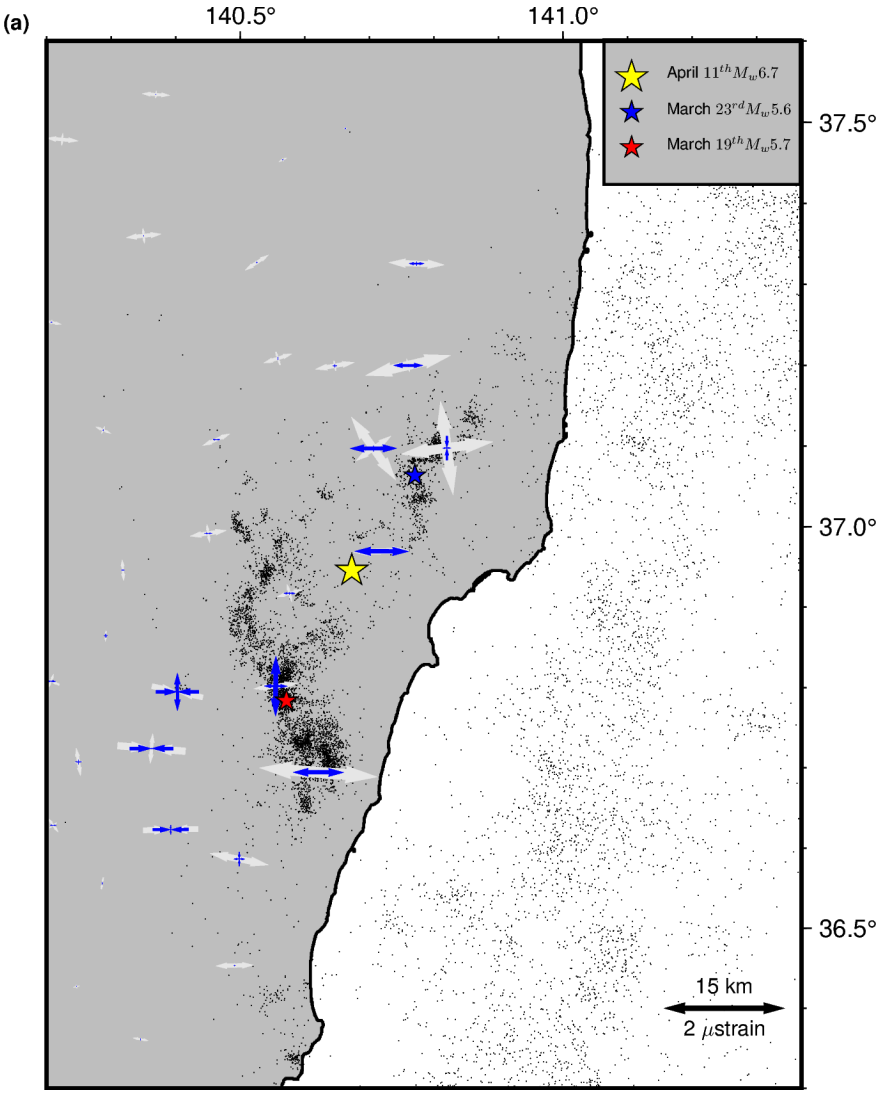

Figure S8. The observed (in white) and modeled (in blue) coseismic free strain in IFPB, taking into account only pre- and post-seismic slips along the faults responsible for the March 19th Mw5.7 earthquake and the March 23rd Mw5.6 earthquake.

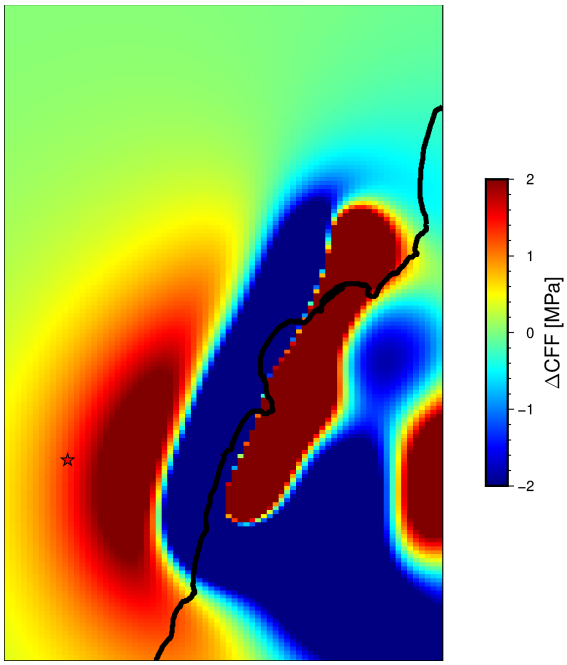

Figure S9. Changes in the CFF along the fault that ruptured during the March 19th Mw5.7 earthquake (strike: 148, dip: 60) due to slip along the low-angle normal fault between March 12th and March 19th(Figure 8a).

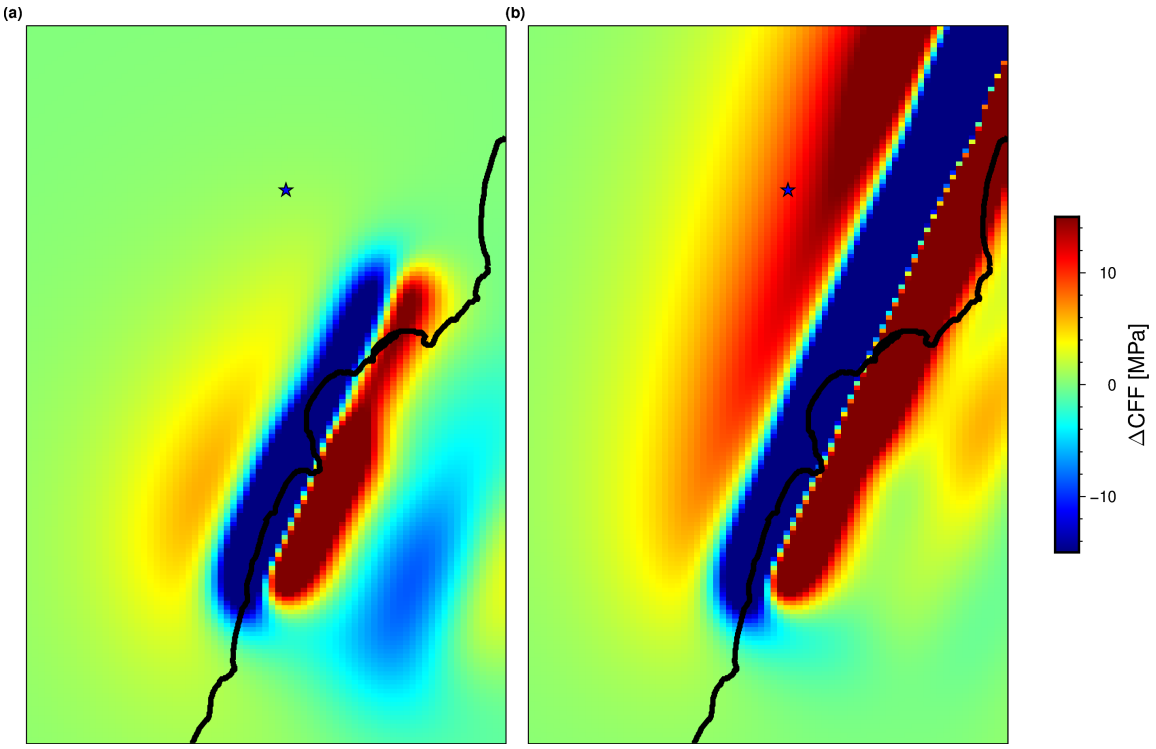

Figure S10. Changes in the CFF along the fault that ruptured during the March 23rd M_w5.6 earthquake (strike: 182, dip: 67) due to slip along the low-angle normal fault. (a) due to slip between March 12th and March 19th (Figure 8a), (b) due to slip between March 19th and March 23rd (Figure 8b).

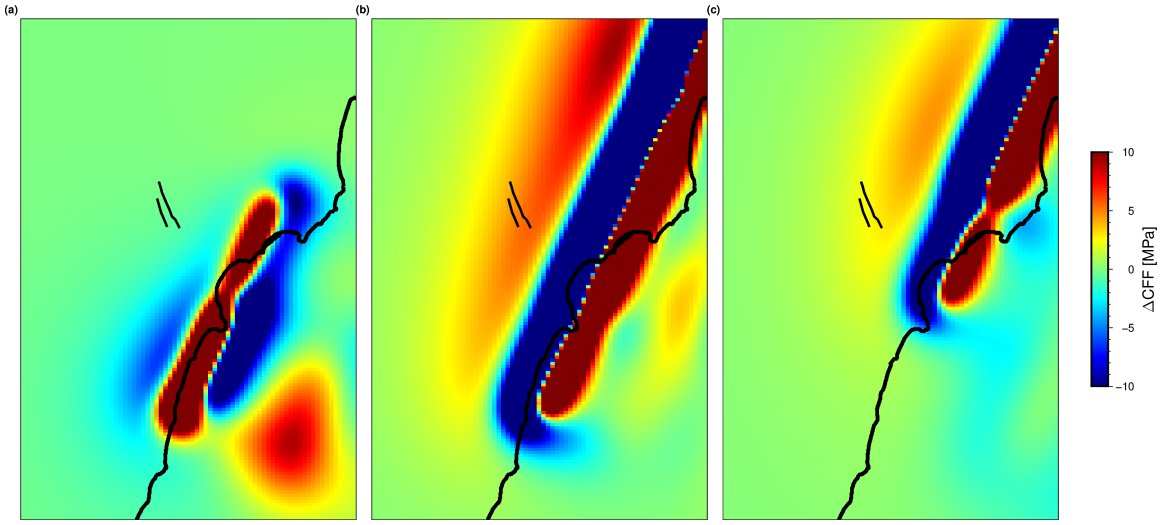

Figure S11. Changes in the CFF along the Itozawa fault that hosted the hypocenter of the April 10th. M_w6.7 Iwaki earthquake (strike: 160, dip: 57) due to slip along the low-angle normal fault. (a) due to slip between March 12th and March 19th (Figure 8a), (b) due to slip between March 19th and March 23rd (Figure 8b), (c) due to slip between March 23rd and April 10th (Figure 8c).

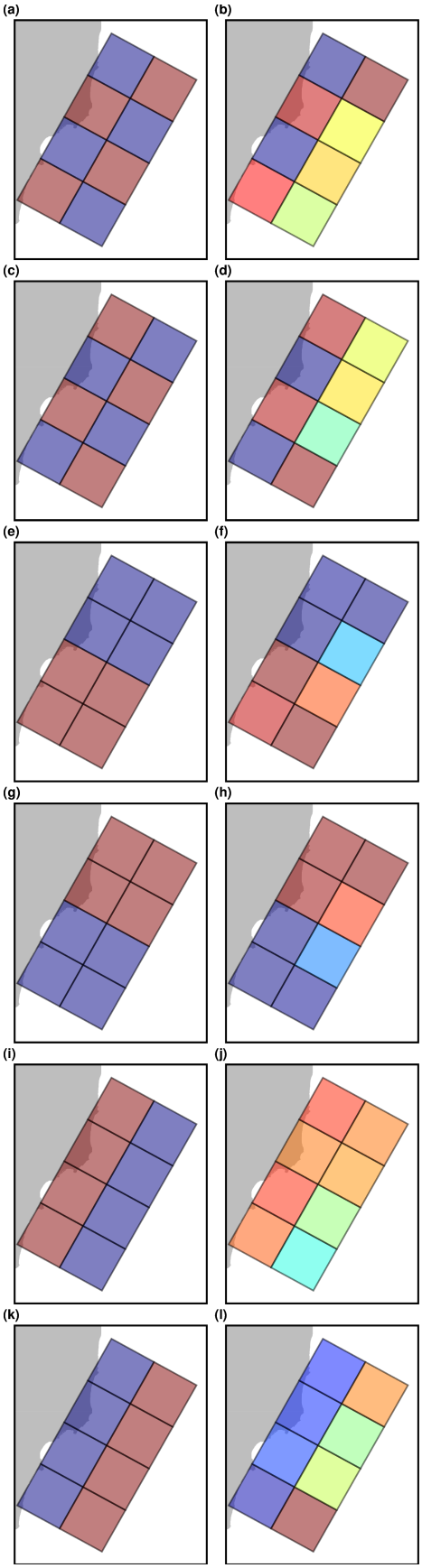

Figure S12.

Checkerboard-style test for resolving low angle normal faults resolution. The left column shows the determined fault slip distribution, from which we calculated synthetic strain data. We added random noise to the synthetic strain data to simulate the uncertainties in the real data (refer to Figure S4 and Table S2). Subsequently, we inverted the noisy synthetic data to obtain the slip along the low angle normal fault, as presented in the right column.

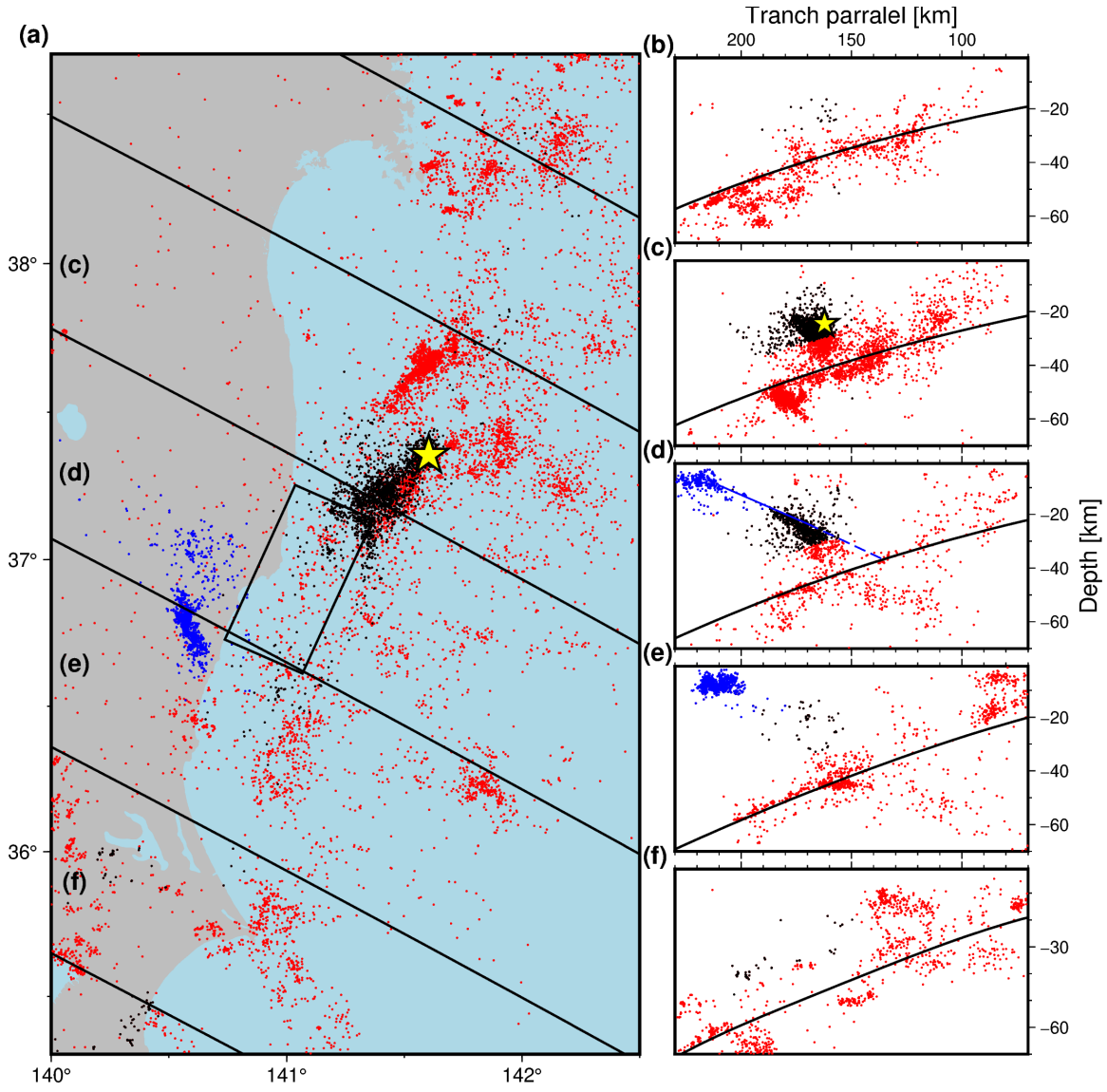

Figure S13

Map showing the distribution of earthquakes with M_w>2 in northeast Japan, which occurred between November 2016 and December 2021. Note the JMA earthquake catalog include information from the ocean bottom S-net during that time span Earthquakes were divided to three groups according to their location. Blue dots indicate primarily on-shore shallow seismicity associated with the IFPB sequence, red dots indicate off-shore events associated with the megathrust, and black dots indicate off-shore off-megathrust earthquakes occurring at depths larger than 20 km. The subduction geometry is from Hayes (2018). (a) Map view of the northeast Japan seismicity. Black lines indicate the location of the trench perpendicular profile presented in panels b-f. (b-f) Trench perpendicular profiles corresponding to the locations in panel a. Yellow star in panels (a) and (c) shows the hypocentral location of the M_w6.9 off-Fukushima normal faulting earthquake.

Supporting Tabels

Table S1. The GEONET stations used in this study. The id column corresponds to the station identifiers found on the Nevada Geodetic Laboratory website (see Open Research section).

id	Longitude	Latitude
I002	140.1743	36.2633
I003	139.8105	36.2037
J041	140.9025	37.0907
J042	140.6118	36.5399
J043	139.7264	36.4018
J201	140.7551	37.5606
J202	140.0727	37.5669
J205	140.6621	37.3255
J209	139.8714	37.2611
J211	140.5616	37.0893
J212	140.4133	36.8621
J213	140.2934	36.6506
J214	140.7539	36.8003
J215	140.0779	36.3649
J216	140.4763	36.3444
J217	140.0393	36.8542
J219	139.9235	36.5989
J561	140.1359	37.4245
J581	140.4976	36.743
J582	139.9878	36.3007
J585	140.1648	36.9523
J586	139.8057	36.9796
J587	139.8543	36.7764
J588	140.1577	36.6925
J590	140.1793	36.5422
J800	140.8416	37.0184
J938	140.5716	37.5911
J939	139.8355	37.4613
J940	140.464	37.4449
J943	140.451	37.2106
J944	140.716	37.1831
J945	140.3763	37.0236
J947	140.3857	36.4759
J948	140.0354	37.1247
J950	139.7528	36.5376

J951	139.9025	36.4566
J965	140.2965	36.779

Table S2. The co-seismic free strain data for the GNSS triplets (refer to Section 2). The columns for longitude and latitude correspond to the centroid location of the respective GNSS triplet. Here, the 1-axis refers to east-west, the 2-axis refers to north-south, and Sexx columns represents the corresponding empirical uncertainties (see Supplementary Text-1 for more details).

id	lon	lat	e11	e22	e12	Se11	Se22	Se12
1	140.773233	37.3256	0.92400282	-0.00536	-0.0386465	0.191127	0.06498075	0.03815749
2	140.662933	37.4924	0.05817405	0.0463284	0.00041603	0.22465968	0.0782916	0.05534603
3	139.899767	36.8700667	0.28399654	0.46269575	-0.044133	0.1054355	0.1305839	0.04402033
4	140.558233	37.2084667	0.42476349	-0.1543988	0.2129469	0.1833484	0.09700049	0.04607446
5	140.318133	36.946	-0.0554283	0.34707606	-0.0325547	0.09955727	0.13984132	0.04157791
6	140.462967	37.1078333	0.40915102	0.04926331	0.19203059	0.15228407	0.12555378	0.04671208
7	140.4504	36.9916667	0.60490254	0.31546557	0.04678435	0.16374849	0.10642284	0.04922014
8	140.576267	36.9172333	0.41321922	0.31641942	0.02958521	0.07201519	0.07545701	0.02572766
9	140.5659	37.4538333	0.13404259	0.07375325	0.03702962	0.22564068	0.08516342	0.06239181
10	140.5257	37.327	0.34613365	0.18518078	0.17875073	0.191949	0.09559924	0.04660762
11	140.3503	37.36	0.58150393	0.26431073	0.03431375	0.14798605	0.0872156	0.0310804
12	140.0147	37.4842333	0.20728722	0.26029542	0.14354354	0.13751783	0.16244722	0.05008259
13	140.369433	37.5343	0.45808633	-0.1132531	-0.038057	0.06579445	0.14392735	0.03227898
14	140.2242	37.4787667	0.53240368	0.21014503	-0.0302037	0.10589856	0.17716725	0.03873813
15	139.9476	37.3823	0.21756361	0.09781559	0.12051448	0.15144155	0.14026872	0.0391905
16	139.939033	36.7431667	0.36710013	0.10349287	-0.0474431	0.14884776	0.08642266	0.04072862
17	140.7602	37.1997667	1.38748511	0.29136412	0.27165874	0.22893951	0.16277257	0.09177147
18	140.646567	37.1993	0.63687767	-0.137259	0.1412065	0.1959771	0.1027166	0.06596099
19	140.207433	37.2532667	0.32545602	0.08589903	-0.0575218	0.1416569	0.10853749	0.03526062
20	140.287567	37.1196333	0.25687923	0.16087195	-0.0507072	0.18928454	0.12399292	0.04824144
21	140.192167	37.0335333	0.04860786	0.44744642	-0.1170895	0.16729232	0.20032562	0.05888406
22	140.014233	37.2701	0.42976811	-0.0194389	0.05652555	0.20180096	0.15472088	0.08712751
23	139.904167	37.1218	0.45448315	-0.2068133	0.10641835	0.37417745	0.11635403	0.05185519
24	140.079833	36.9770667	0.62790738	0.43621909	-0.0381872	0.26633434	0.13797247	0.09948812
25	139.960133	36.9861667	0.35850779	0.39984651	-0.0251	0.18962628	0.14051755	0.06429192
26	139.843533	36.6376333	0.35230217	-0.0739959	-0.0767985	0.14280978	0.08790484	0.04360732
27	139.804267	36.7645333	0.24234422	0.12774221	-0.0112273	0.36614118	0.06304078	0.03513932
28	139.9894	36.3740667	0.27821732	0.19535436	0.01846407	0.12297941	0.12750348	0.04487597
29	139.7939	36.4653333	0.46842842	0.43244868	-0.0483165	0.11582454	0.14596729	0.04850716
30	139.8596	36.5310333	0.32659583	0.01907703	-0.1033636	0.12094584	0.14325349	0.03967845
31	139.813133	36.3540333	0.55960037	-0.0031245	0.01150513	0.14185692	0.07719957	0.03063674
32	139.900267	36.3203333	0.22248483	-0.0121415	0.02128395	0.11153789	0.08466137	0.03293898
33	140.08	36.3096333	0.3029191	0.19549149	0.06058883	0.12747925	0.18699388	0.04920582
34	139.990867	36.2559	0.32441652	-0.2993329	0.01597608	0.07600268	0.22141894	0.04430541
35	140.554933	36.8018	0.72184214	-0.0008333	0.09503518	0.06743289	0.17927789	0.03540958
36	140.291533	36.8644667	-0.0202563	0.17990792	0.01600091	0.1116202	0.16941825	0.04542802
37	140.402467	36.7947	-0.8220154	-0.0588894	0.1773092	0.11542726	0.1933449	0.05022507
38	140.3625	36.7242	-1.1161058	0.4856982	0.1328695	0.11111414	0.27112176	0.04944554
39	140.040167	36.7152	0.05699062	0.06830156	0.09591859	0.08618885	0.08258354	0.02968148
40	140.2492	36.7073667	0.14748227	0.45357851	-0.0486132	0.13645707	0.26005126	0.06500053
41	140.1206	36.833	0.41229147	0.16520978	0.2089225	0.18107024	0.0740864	0.03057602
42	140.206333	36.8079333	-0.2228167	0.17753949	0.19539737	0.14979982	0.07970144	0.03205382
43	140.820033	37.0974	1.5437843	1.56277155	-0.0026068	0.19720048	0.17864473	0.08229182

44	140.719033	36.9693333	0.93655664	0.04835117	0.02722919	0.09738614	0.0737754	0.03417828
45	140.7064	37.0969333	0.8981458	1.08874289	-0.2668055	0.09339604	0.1627941	0.04366785
46	140.345433	36.3612	0.25279837	-0.0153707	-0.0478728	0.08240551	0.10235271	0.03650871
47	140.392233	36.6231667	-0.9094357	0.01856614	-0.0229525	0.1683109	0.07618012	0.04539764
48	140.143833	36.3901333	0.11147351	-0.053733	0.04272833	0.21517353	0.10887887	0.03684281
49	140.246433	36.4271333	0.10187265	-0.052076	0.03596676	0.10620824	0.10258947	0.03718678
50	140.286133	36.5562333	0.03171768	-0.1845746	-0.0397293	0.12243913	0.18672445	0.05205792
51	140.210133	36.6284333	0.00507158	0.13991095	-0.2057714	0.18126653	0.16834528	0.0574227
52	140.086833	36.6112	0.20079422	0.19694745	-0.1073366	0.06573007	0.15779898	0.03699263
53	140.053233	36.4545667	0.26974159	-0.1103788	-0.0571402	0.0856276	0.13139925	0.03448904
54	140.001767	36.5325667	0.24607756	-0.0409806	-0.1030449	0.07124941	0.14712665	0.04372549
55	140.491267	36.4534	0.62946642	0.07884118	0.01348442	0.1285585	0.11549392	0.04863233
56	140.498367	36.5862667	0.95420888	0.06013991	-0.1834878	0.13717096	0.07325193	0.0302353
57	140.6211	36.6944	1.94747841	-0.0404086	-0.1533376	0.09387104	0.11534693	0.03348369